ACS APPLIED MATERIALS & INTERFACES

Letter

www.acsami.org

Magnetron Sputtered Zinc Oxide Nanorods as Thickness-Insensitive Cathode Interlayer for Perovskite Planar-Heterojunction Solar Cells

Lusheng Liang,[†,‡] Zhifeng Huang,[†] Longhua Cai,[‡] Weizhong Chen,[‡] Baozeng Wang,[‡] Kaiwu Chen,[‡] Hua Bai,*[,†] Qingyong Tian,*[,‡] and Bin Fan*[,‡]

[†]College of Materials, Xiamen University, Xiamen 361005, P. R. China

[‡]Weihua Solar Co. Ltd., Xiamen 361115, P. R. China

Supporting Information

ABSTRACT: Suitable electrode interfacial layers are essential to the high performance of perovskite planar heterojunction solar cells. In this letter, we report magnetron sputtered zinc oxide (ZnO) film as the cathode interlayer for methylammonium lead iodide ($CH_3NH_3PbI_3$) perovskite solar cell. Scanning electron microscopy and X-ray diffraction analysis demonstrate that the sputtered ZnO films consist of *c*-axis aligned nanorods. The solar cells based on this ZnO cathode interlayer showed high short circuit current and power conversion efficiency. Besides, the performance of the device is insensitive to the thickness of ZnO cathode interlayer. Considering the high reliability and maturity of sputtering technique both in lab and industry, we believe that the sputtered ZnO films are promising cathode interlayers for perovskite solar cells, especially in large-scale production.

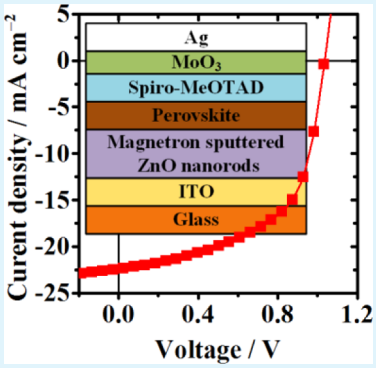

KEYWORDS: *short circuit current, flexible solar cell, electron transport layer*

The last five years have witnessed rapid development of solar cells based on organic−inorganic hybrid perovskite materials,[1−3] because of their large absorption coefficient and long charge carrier diffusion length,[4,5] which lead to high power conversion efficiency (PCE) of more than 19%.[6] Recent reports revealed that methylammonium lead halide ($CH_3NH_3PbX_3$) perovskite can be deposited from solution at low temperature, and thus it is possible to fabricate perovskite-based solar cell with roll-to-roll technique, which is the lowest-cost method for producing thin film solar cell.[7,8]

There are two basic types of perovskite thin film solar cell, namely, mesoporous scaffold solar cell (MSSC) and planar heterojunction solar cell (PHJSC). In MSSCs, mesoporous metal oxides, such as Al_2O_3,[9] ZrO_2,[10] TiO_2,[11] and NiO,[12] are used as scaffold for perovskite active layer, whereas in PHJSCs, a pure perovskite layer is sandwiched between anode and cathode interlayers.[6,7,13,14] High efficiencies up to 16.7% were obtained in MSSCs.[15] However, the fabrication process of mesoporous scaffold is relatively complicated, and usually requires high temperature, which may damage the polymer substrate commonly used in roll-to-roll technique. PHJSCs have simple structure, and are able to avoid the use of high temperature, and thus are easy to fabricate with lower energy consuming.

In PHJSC, the photoexcitons generated in perovskite layer diffuse to the cathode or anode interface and separate there. And since perovskite has low exciton binding energy (37 to 50 meV), which is comparable to thermal energies, there are also plenty of free charges in perovskite layer.[16,17] Therefore, the cathode interlayer in PHJSC must be both electron transport layer and hole block layer. TiO_2 is the most widely used cathode interlayer.[6,13] The PHJSC with TiO_2 as cathode interlayer and 2,2′,7,7′-tetrakis[N,N-di(4-methoxyphenyl)-amino]-9,9′-spirobifluorene (spiro-MeOTAD) as cathode interlayer showed a high PCE of 19.3%.[6] ZnO is an alternative to TiO_2, because of its suitable energy levels and good electron transport properties.[18−21] With compact ZnO as cathode interlayer, a perovskite PHJSC with a PCE of 15.7% has been reported.[22] However, for both TiO_2 and ZnO interlayer, their thickness strongly influences the performance of the devices. For example, Liu et al. investigated the effect of the thickness of ZnO cathode interlayer on the performance of the device, and found that when the thickness of ZnO increased from 25 to 70 nm, the PCE of the device decreased by ∼10%.[22] The dependence of cell performance on interlayer thickness requires precise deposition of the interlayer. Besides, TiO_2 or ZnO cathode interlayers were usually deposited from nanoparticle suspension,[22] or precursor solutions.[13] These processes are complicated, involving the preparation of well-dispersed nanoparticles, or post thermal treatment to promote the conversion of precursor. Herein, we report magnetron sputtered ZnO film as cathode interlayer for perovskite PHJSCs. Magnetron sputter is a simple and reliable technique, which is widely used both in laboratory and industry, to prepare

Received: October 1, 2014
Accepted: November 18, 2014
Published: November 18, 2014

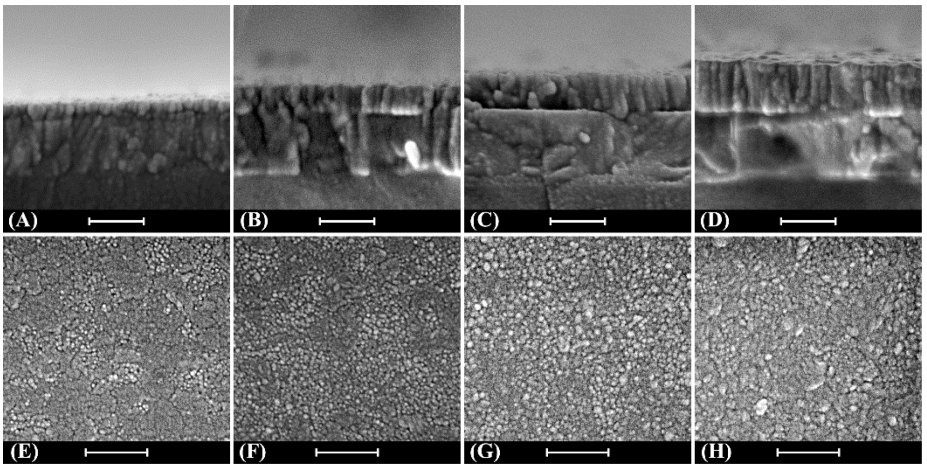

Figure 1. SEM images of magnetron sputtered (A, E) ZnO-1, (B, F) ZnO-2, (C, G) ZnO-3, and (D, H) ZnO-4 films. (A–D) Section view, scale bar 200 nm; (E, F) top view, scale bar 500 nm.

high-quality thin films. The commonly used metal oxide transparent electrodes, such as ITO (indium tin oxide), are fabricated by magnetron sputter technique. Therefore, the sputtering of ITO and ZnO film can be carried out sequentially, which is valuable to the future large-scale production of solar cells in industry. We found that the magnetron sputtered ZnO film consisted of aligned ZnO nanorods. The devices based on this ZnO interlayer had high short circuit current and PCE, and their performance was insensitive to the thickness of ZnO interlayer. Furthermore, our cathode interlayer is compatible to flexible devices, because the deposition of ZnO does not require high temperature. The flexible solar cells based on magnetron sputtered ZnO interlayer were fabricated and they also showed high PCE.

Figure 1 shows the morphologies of ZnO films on ITO glass prepared by magnetron sputtering with different deposition time. From ZnO-1 to ZnO-4, the sputtering time was 8, 15, 22, and 29 min, respectively. In the cross-sectional SEM images, it is found that the ZnO films consist of nanorods array. The diameter of the ZnO nanorods is 50–80 nm. This is a typical

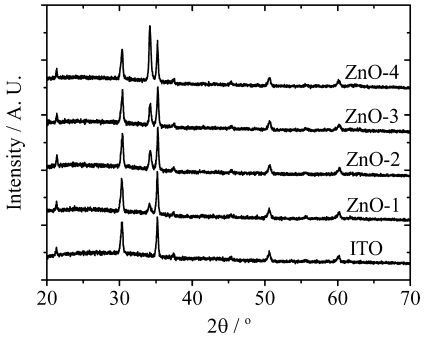

Figure 2. XRD patterns of ITO glass substrate and different ZnO films.

structure of sputtered ZnO thin film, usually obtained when the temperature of the substrate is low.[23] In our sputtering experiments, the temperature of the substrate was about 100 °C. At such a low substrate temperature, the motion of adatoms is frozen, thus ZnO can only grow in normal direction, and surface diffusion between grains is strongly limited.[24] The thickness of the ZnO films are 40, 80, 120, and 160 nm, as

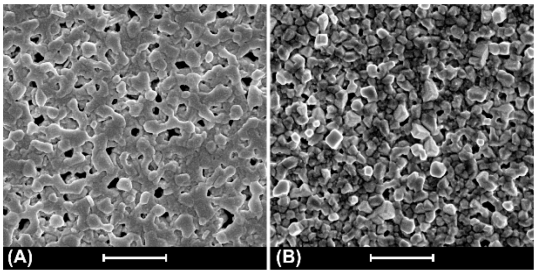

Figure 3. SEM images of (A) PbI_2 and (B) $CH_3NH_3PbI_3$ perovskite films. Scale bar: 1 μm.

measured by SEM images, for ZnO-1, -2, -3, and -4, respectively. Thus, the thickness of the ZnO film is proportional to sputtering time, and by changing sputtering time, we can control the thickness of ZnO film, without altering the structure of the film. The top-view SEM images of the ZnO films show irregular packed particles with diameter of several tens of nanometers, and with the increase of sputter time, the particle size became slightly larger. The crystalline structures of ZnO films were investigated with X-ray diffraction (XRD). As depicted in Figure 2, in the XRD patterns of ZnO films, there is a peak at 2θ = 34.2°, whose intensity increases with the thickness of the film. This is the characteristic peak of *c*-axis oriented ZnO, corresponding to (002) plane reflection.[25,26] Other diffraction peaks of ZnO are not detectable in our samples, showing that almost all hexagonal zincite crystallites are perpendicular to the ITO substrate.[25] The XRD results agree well with the rodlike morphology of ZnO film shown in Figure 1, and both of them demonstrate that the ZnO films were deposited on ITO with preferred orientation.

With ZnO-1 film as cathode interlayer, inverse PHJSC devices were fabricated. $CH_3NH_3PbI_3$ was directly deposited onto the ZnO layer following a two stepped procedure.[27] PbI_2 was first spin-coated onto ZnO surface, then the PbI_2-coated ITO glass was dipped in a solution of CH_3NH_3I in 2-propanol for 2 min, rinsed with 2-propanol and then dried under a flow of clean air. The morphology of the as-prepared PbI_2 film is represented in Figure 3A. The film consists of interconnected and irregular particles, which are believed to be PbI_2-DMF complex, because DMF molecules are difficult to remove from the film at low temperature.[28] There were some pinholes in PbI_2 film, whose diameter is around 200–300 nm. However,

dx.doi.org/10.1021/am506672j | ACS Appl. Mater. Interfaces 2014, 6, 20585–20589

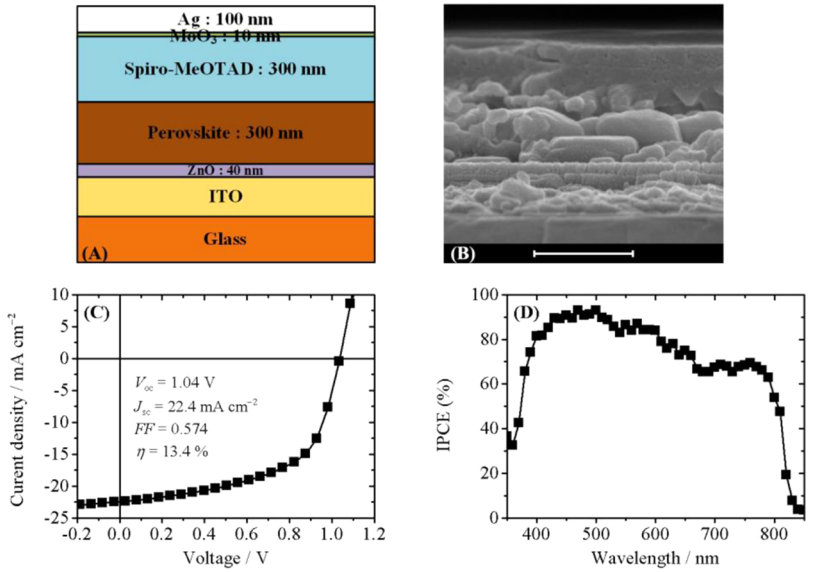

Figure 4. Structure and performance of the perovskite solar cell. (A) Structure of the solar cell. (B) Cross-sectional SEM image of the solar cell. (C) Current−voltage (J−V) curve measured under AM 1.5 solar light. (D) IPCE spectrum.

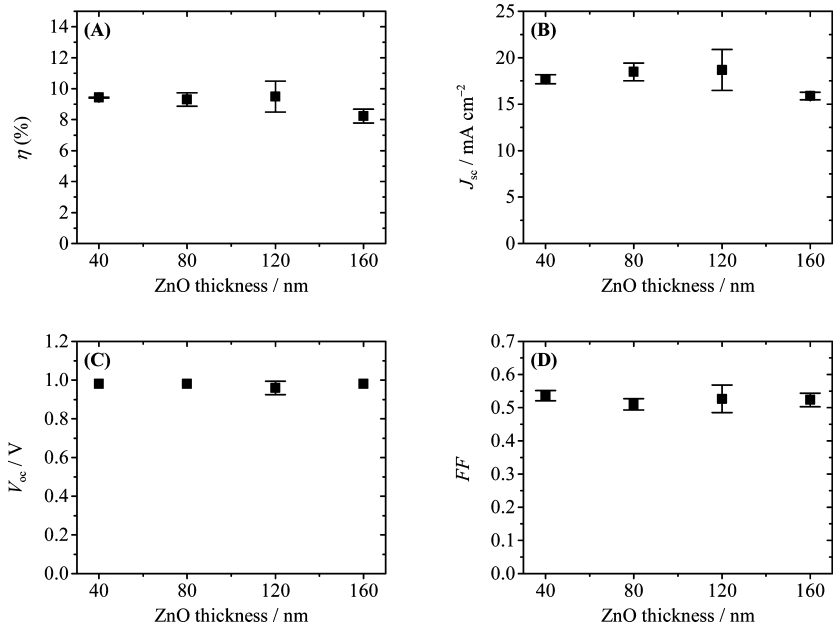

Figure 5. Performance of devices with different ZnO films. (A) Power conversion efficiency, (B) short circuit current, (C) open circuit voltage, and (D) fill factor.

Table 1. Sheet Resistance of ITO and ZnO-Coated ITO

entry	description	thickness of ZnO (nm)	sheet resistance (Ω/□)
1	glass/ITO	0	8.0
2	glass/ITO/ZnO-1	40	5.9
3	glass/ITO/ZnO-2	80	5.9
4	glass/ITO/ZnO-3	120	6.5
5	glass/ITO/ZnO-4	160	6.9

most of these pinholes disappeared after the reaction with CH_3NH_3I, as shown in Figure 3B. Moreover, the morphology of the film also changed: the surface of the film was covered by crystals with diameter of 100−200 nm. It should be noted here that the DMF molecules and pinholes existing in PbI_2 film may help in the formation of $CH_3NH_3PbI_3$, via promoting the diffusion of CH_3NH_3I in the film and inside the crystalline grain. The conversion of PbI_2 to $CH_3NH_3PbI_3$ was confirmed by obvious color change, from yellow to dark brown. Onto the $CH_3NH_3PbI_3$ layer, spiro-MeOTAD was spin-coated as the hole transport layer, and a thin layer of MoO_3 was then deposited by evaporation to improve the interface charge transfer (the effect of MoO_3 on the performance of the device is shown in Figure S1 in the Supporting Information). Finally, silver was evaporated as the anode. The structure and the cross-sectional image of the device are shown in Figure 4A, B.

The performance of the devices with different ZnO interlayers was measured under AM 1.5 condition. The current−voltage (J−V) curve of the highest-performing device with ZnO-1 as cathode interlayer is depicted in Figure 4C. (histogram of efficiency for 80 devices can be found in Figure

dx.doi.org/10.1021/am506672j | ACS Appl. Mater. Interfaces 2014, 6, 20585−20589

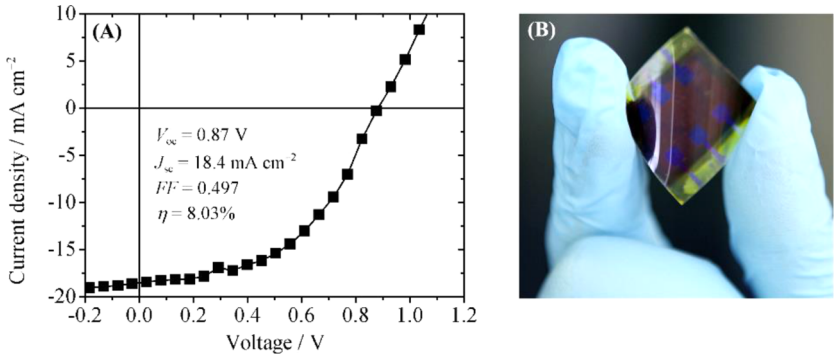

Figure 6. (A) Current−voltage (J−V) curve measured under AM 1.5 solar light and (B) the photograph of flexible device on PET substrate.

S2 in the Supporting Information) The devices showed hysteresis behaviors, that is, the performance was dependent on the scan direction and scan rate of the J−V measurement. The details are depicted in the Supporting Information (Figure S3). Unless stated otherwise, the scan direction was from short circuit to forward bias, and measurement time for each data point was 500 ms. The short circuit current (J_{sc}), open circuit voltage (V_{oc}), fill factor and PCE of the device were measured as 22.4 mA cm^{-2}, 1.04 V, 57.4% and 13.4%. The Jsc value is larger than that of the device with ZnO nanoparticles as cathode interlayer (20.4 mA cm^{-2}),[22] and also larger than those of devices with compact (21.5 mA cm^{-2})[29] or mesoporous TiO_2 cathodes (20.0 mA cm^{-2}).[30] These results reveal that magnetron sputtered ZnO are good electron acceptor and electron conductor. However, the fill factor of the device is relatively low, probably due to the defects and pinholes in the perovskite layer, as shown in Figure 3B. These defects lead to poor contact between perovskite and ZnO, diminishing the performance of the devices. It should be noted that in the present work, we did not optimize the preparation procedure of $CH_3NH_3PbI_3$ layer, thus we believe the quality of $CH_3NH_3PbI_3$ layer and the performance of the solar cell can be improved, if further optimization is carried out. The incident photon-to-electron conversion efficiency (IPCE) spectrum of the device is represented in Figure 4D. Between 400 to 700 nm, the IPCE spectra shows a broad plateau from 70 to 90%, which is the characteristic of devices based on $CH_3NH_3PbI_3$. Integrating the product of the AM1.5G photon flux with the IPCE spectrum yields a predicted J_{sc} of 21.1 mA cm^{-2}, which is in good agreement with the measured value of 22.4 mA cm^{-2}. After 900 h, the PCE of the device decreased to 8.5%, showing good stability (see Figure S4 in the Supporting Information). However, we believe the stability of the ZnO based device can be further improved if spiro-MeOTAD can be replaced by a more stable anode interlayer material.

We further investigated the effect of ZnO thickness on the performance of the device. As shown in Figure 5, when the thickness of ZnO cathode interlayer increases from 40 to 160 nm, the performance of the devices changes very little. This property of sputtered ZnO interlayer is attractive, because it significantly reduce the difficulty of fabricating solar cell devices. This phenomenon can be ascribed to the uniform growth and high conductivity of magnetron sputtered ZnO film. As shown above, the crystal structure of ZnO film is independent of the thickness, and thus the work functions of different ZnO films should be identical. Consequently, these devices showed the same V_{oc} values. We also measured the sheet resistance of ZnO coated ITO samples. As shown in Table 1, after deposition of 40 nm thick ZnO, the sheet resistance of ITO decreases from 8.0 Ω/□ to 5.9 Ω/□. Further increasing the thickness of ZnO layer results in slightly increment in sheet resistance, but the values are still smaller than bare ITO even the thickness of ZnO layer reach 160 nm. These results reveal that the magnetron sputtered ZnO on ITO substrate have good electric conductivity, which can be explained by the oriented growth of ZnO nanorods. Because *c*-axis oriented ZnO nanorods are perpendicular to the ITO substrate, the transport of electrons along the *c*-axis (across the ZnO film) will be seldom scattered by grain boundary, and consequently electrons generated in the bulk perovskite or at the ZnO/perovskite interface can be easily conducted to ITO electrode. Therefore, the thickness of ZnO layer has little effect on the photovoltaic performance of the device.

Because the sputtered ZnO cathode interlayer do not require high temperature thermal processing, it can be used in flexible devices with plastics substrate. Figure 6 depicts the photograph and J−V curve of the flexible device on ITO-coated poly(ethylene terephthalate) (PET) with sputtered ZnO as cathode interlayer. The J−V curve of the highest-performing device yields a V_{oc} of 0.87 V, a J_{sc} of 18.4 mA cm^2, a fill factor of 49.7%, and a PCE of 8.03%. The performance of the flexible device is lower than that on glass substrate. A possible reason is the nonuniformity of perovskite layer and/or hole transport layer, due to slight deformation of PET substrate during spin-coating process of perovskite. The nonuniform perovskite layer contains more defects, which may lead to recombination of charges. However, these results can still demonstrate that magnetron sputtered ZnO cathode interlayer is suitable for flexible perovskite devices.

In conclusion, we have fabricated planar perovskite solar cells with magnetron sputtered ZnO film as cathode interlayer. The sputtered ZnO films consist of *c*-axis oriented ZnO nanorods perpendicular to the ITO substrate. Devices based on ZnO nanorods cathode interlayer show high J_{sc} and good *PCE*, and their performance is insensitive to the thickness of ZnO layer. This is ascribed to the high electric conductivity of ZnO along *c*-axis. Flexible device with sputtered ZnO film as cathode interlayer also has good performance. Considering the high reliability and maturity of sputtering technique both in lab and industry, we believe that the sputtered ZnO film is a promising cathode interlayer for perovskite solar cell, especially in large-scale production.

■ ASSOCIATED CONTENT

Supporting Information

Details of experiments and additional figures as described in the text. This material is available free of charge via the Internet at http://pubs.acs.org.

■ AUTHOR INFORMATION

Corresponding Authors

*E-mail: baihua@xmu.edu.cn.
*E-mail: tianqingyong@weihua-solar.com.
*E-mail: fanbin@weihua-solar.com.

Notes

The authors declare no competing financial interest.

■ REFERENCES

(1) Kojima, A.; Teshima, K.; Shirai, Y.; Miyasaka, T. Organometal Halide Perovskites as Visible-Light Sensitizers for Photovoltaic Cells. *J. Am. Chem. Soc.* **2009**, *131*, 6050−6051.

(2) Park, N. G. Organometal Perovskite Light Absorbers toward a 20% Efficiency Low-Cost Solid-State Mesoscopic Solar Cell. *J. Phys. Chem. Lett.* **2013**, *4*, 2423−2429.

(3) Snaith, H. J. Perovskites: The Emergence of a New Era for Low-Cost, High-Efficiency Solar Cells. *J. Phys. Chem. Lett.* **2013**, *4*, 3623−3630.

(4) Stranks, S. D.; Eperon, G. E.; Grancini, G.; Menelaou, C.; Alcocer, M. J. P.; Leijtens, T.; Herz, L. M.; Petrozza, A.; Snaith, H. J. Electron-Hole Diffusion Lengths Exceeding 1 Micrometer in an Organometal Trihalide Perovskite Absorber. *Science* **2013**, *342*, 341−344.

(5) Xing, G.; Mathews, N.; Sun, S.; Lim, S. S.; Lam, Y. M.; Gräetzel, M.; Mhaisalkar, S.; Sum, T. C. Long-Range Balanced Electron and Hole-Transport Lengths in Organic-Inorganic $CH_3NH_3PbI_3$. *Science* **2013**, *342*, 344−347.

(6) Zhou, H.; Chen, Q.; Li, G.; Luo, S.; Song, T. B.; Duan, H. S.; Hong, Z.; You, J.; Liu, Y.; Yang, Y. Photovoltaics Interface Engineering of Highly Efficient Perovskite Solar Cells. *Science* **2014**, *345*, 542−546.

(7) You, J. B.; Hong, Z. R.; Yang, Y.; Chen, Q.; Cai, M.; Song, T. B.; Chen, C. C.; Lu, S.; Liu, Y.; Zhou, H.; Yang, Y. Low-Temperature Solution Processed Perovskite Solar Cells with High Efficiency and Flexibility. *ACS Nano* **2014**, *2*, 1674−1680.

(8) Wojciechowsk, K.; Saliba, M.; Leijtens, T.; Abate, A.; Snaith, H. J. Sub-150 Degrees C Processed Meso-Superstructured Perovskite Solar Cells with Enhanced Efficiency. *Energy Environ. Sci.* **2014**, *7*, 1142−1147.

(9) Lee, M. M.; Teuscher, J.; Miyasaka, T.; Murakami, T. N.; Snaith, H. J. Efficient Hybrid Solar Cells Based on Meso-Superstructured Organometal Halide Perovskites. *Science* **2012**, *338*, 643−647.

(10) Bi, D. Q.; Moon, S. J.; Häeggman, L.; Boschloo, G.; Yang, L.; Johansson, E. M. J.; Nazeeruddin, M. K.; Gräetzel, M.; Hagfeldt, A. Using a Two-Step Deposition Technique to Prepare Perovskite ($CH_3NH_3PbI_3$) for Thin Film Solar Cells Based on ZrO_2 and TiO_2 Mesostructures. *RSC Adv.* **2013**, *3*, 18762−18766.

(11) Kim, H. S.; Lee, C. R.; Im, J. H.; Lee, K. B.; Moehl, T.; Marchioro, A.; Moon, S. J.; Humphry B, R.; Yum, J. H.; Moser, J. E.; Grätzel, M.; Park, N. G. Lead Iodide Perovskite Sensitized All-Solid-State Submicron Thin Film Mesoscopic Solar Cell with Efficiency Exceeding 9%. *Sci. Rep.* **2012**, *2*, 591.

(12) Wang, K. C.; Jeng, J. Y.; Shen, P. S.; Chang, Y. C.; Diau, E. W. G; Tsai, C. H.; Chao, T. Y.; Hsu, H. C.; Lin, P. Y.; Chen, P.; Guo, T. F.; Wen, T. C. p-Type Mesoscopic Nickel Oxide/Organometallic Perovskite Heterojunction Solar Cells. *Sci. Rep.* **2014**, *4*, 4756.

(13) Eperon, G. E.; Burlakov, V. M.; Docampo, P.; Goriely, A.; Snaith, H. J. Morphological Control for High Performance, Solution-Processed Planar Heterojunction Perovskite Solar Cells. *Adv. Funct. Mater.* **2014**, *24*, 151−157.

(14) Malinkiewicz, O.; Yella, A.; Lee, Y. H.; Espallargas, G. M.; Gräetzel, M.; Nazeeruddin, M. K.; Bolink, H. J. Perovskite Solar Cells Employing Organic Charge-Transport Layers. *Nat. Photonics* **2014**, *2*, 128−132.

(15) Jeon, N. J.; Lee, H. G.; Kim, Y. C.; Seo, J.; Noh, J. H.; Lee, J.; Seok, S. I. o-Methoxy Substituents in Spiro-OMeTAD for Efficient Inorganic-Organic Hybrid Perovskite Solar Cells. *J. Am. Chem. Soc.* **2014**, *22*, 7837−7840.

(16) Tanaka, K.; Takahashi, T.; Ban, T.; Kondo, T.; Uchida, K.; Miura, N. Comparative Study on the Excitons in Lead-Halide-Based Perovskite-type Crystals $CH_3NH_3PbBr_3CH_3NH_3PbI_3$. *Solid State Commun.* **2003**, *127*, 619−623.

(17) Hirasawa, M.; Ishihara, T.; Goto, T.; Uchida, K3.; Miura, N. Magnetoabsorption of the Lowest Exciton in Perovskite-Type Compound $(CH_3NH_3)PbI_3$. *Phys. B* **1994**, *201*, 427−430.

(18) Bi, D. Q.; Boschloo, G.; Schwarzmueller, S.; Yang, L.; Johansson, E. M. J.; Hagfeldt, A. Efficient and Stable $CH_3NH_3PbI_3$-Sensitized ZnO Nanorod Array Solid-State Solar Cells. *Nanoscale* **2013**, *5*, 11686−11691.

(19) Kumar, M. H.; Yantara, N.; Dharani, S.; Gräetzel, M.; Mhaisalkar, S.; Boix, P. P.; Mathews, N. Flexible, Low-Temperature, Solution Processed ZnO-Based Perovskite Solid State Solar Cells. *Chem. Commun.* **2013**, *49*, 11089−11091.

(20) Ramos, F. J.; Santos, M. C. L.; Guillén, E.; Nazeeruddin, M. K.; Grätzel, M.; Gonzalez-Elipe, A. R.; Ahmad, S. Perovskite Solar Cells Based on Nanocolumnar Plasma-Deposited ZnO Thin Films. *ChemPhysChem* **2014**, *15*, 1148−1153.

(21) Do, K.; Choi, H.; Lim, K.; Jo, H.; Cho, J. W.; Nazeeruddin, M. K.; Ko, J. Star-Shaped Hole Transporting Materials with a Triazine Unit for Efficient Perovskite Solar Cells. *Chem. Commun.* **2014**, *50*, 10971−10974.

(22) Liu, D. Y.; Kelly, T. L. Perovskite Solar Cells with a Planar Heterojunction Structure Prepared Using Room-Temperature Solution Processing Techniques. *Nat. Photonics* **2014**, *8*, 133−138.

(23) Sundaram, K. B.; Khan, A. Characterization and Optimization of Zinc Oxide Films by RF Magnetron Sputtering. *Thin Solid Films* **1997**, *295*, 87−91.

(24) Ohring, M. *Material Science of Thin Films: Depostion and Structure*, 2nd ed; Elsevier: N J, 2002.

(25) Takada, S. Relation between Optical Property and Crystallinity of ZnO Thin Films Prepared by RF Magnetron Sputtering. *J. Appl. Phys.* **1993**, *73*, 4739−4742.

(26) Akhtar, N.; Polyakov, A. O.; Aqeel, A.; Gordiichuk, P.; Blake, G. R.; Baas, J.; Amenitsch, H.; Herrmann, A.; Rudolf, P.; Palstra, T. T. M. Self-Assembly of Ferromagnetic Organic-Inorganic Perovskite-Like Films. *Small* **2014**, DOI: 10.1002/smll.201400259.

(27) Burschka, J.; Pellet, N.; Moon, S. J.; Humphry-Baker, R.; Gao, P.; Nazeeruddin, M. K.; Grätzel, M. Sequential Deposition as a Route to High-Performance Perovskite-Sensitized Solar Cells. *Nature* **2013**, *499*, 316−319.

(28) Wakamiya, A.; Endo, M.; Sasamori, T.; Tokitoh, N.; Ogomi, Y.; Hayase, S.; Murata, Y. Reproducible Fabrication of Efficient Perovskite-Based Solar Cells: X-Ray Crystallographic Studies on the Formation of $CH_3NH_3PbI_3$ Layers. *Chem. Lett.* **2014**, *43*, 711−713.

(29) Liu, M. Z.; Johnston, M. B.; Snaith, H. J. Efficient Planar Heterojunction Perovskite Solar Cells by Vapour Deposition. *Nature* **2013**, *501*, 395−398.

(30) Burschka, J.; Pellet, N.; Moon, S. J.; Humphry-Baker, R.; Gao, P.; Nazeeruddin, M. K.; Gräetzel, M. Sequential Deposition as a Route to High-Performance Perovskite-Sensitized Solar Cells. *Nature* **2013**, *499*, 316−319.